CrossMark

ORIGINAL ARTICLE

Influence of operational parameters on photocatalytic amitrole degradation using nickel organic xerogel under UV irradiation

**Miguel A. Álvarez [a], Francisco Orellana-García [a], M. Victoria López-Ramón [a,*],
José Rivera-Utrilla [b], Manuel Sánchez-Polo [b]**

[a] *Department of Inorganic and Organic Chemistry, Faculty of Experimental Science, University of Jaen, 23071 Jaen, Spain*
[b] *Department of Inorganic Chemistry, Faculty of Science, University of Granada, 18071 Granada, Spain*

Abstract   The objectives of this study were to analyze the influence of different operational variables and to determine the time course of total organic carbon (TOC) and medium toxicity during amitrole (AMT) photodegradation in the presence of Ni xerogel (X-Ni) as photocatalyst. A further study objective was to analyze the influence of the type of water on the photodegradation process. Results show that the degradation rate is directly proportional to the initial X-Ni concentration up to a maximum of 250 mg/L with a slight decrease thereafter, indicating progressive photon absorption saturation of the catalyst for a given incident radiation flow. At concentrations close to 250 mg/L X-Ni, the AMT photodegradation rate is not affected by further increases in X-Ni concentration. In addition, AMT photolysis is highly pH-dependent and is generally favored at pH values at which AMT is in its ionic form. The increase observed in AMT degradation rate under alkaline conditions can be attributed to the higher generation of HO· radicals. The presence of chloride reduces the AMT degradation rate, because Cl^- anions behave as h^+ and HO· radical scavengers. The degradation rate is also decreased by addition to the medium of organic matter, which acts as a filter. The behavior of TOC removal kinetics during AMT degradation in the presence of X-Ni is similar to that observed for AMT degradation kinetics. Finally, we highlight that photocatalysis is more effective in ultrapure water than in wastewater or tap water. In all systems, the optimal catalyst concen-

Production and hosting by Elsevier

tration is 250 mg/L. The medium toxicity increases with longer treatment time, indicating the formation of by-products that are smaller than AMT and can more readily penetrate the cell.

1. Introduction

Amitrole (AMT) is a non-selective herbicide with a very wide spectrum of activity against annual and perennial broad leaf and grass type weeds. It is sometimes used instead of prohibited herbicides and is extensively employed for weed control in agriculture and along roadsides and railways (Catastini et al., 2004; Da Pozzo et al., 2005; Oesterreich et al., 1999). Due to its high solubility, relatively high AMT levels can be found in surface water and contribute to groundwater contamination *via* leaching. AMT has been reported to be an endocrine disruptor and possible carcinogen (Andersen et al., 2013; Da Pozzo et al., 2005; Mugadza and Nyokong, 2010; Watanabe et al., 2005). Increasingly strict environmental restrictions in the presence of these compounds in effluents and natural systems require treatment technologies that minimize environmental risks at a reasonable cost.

Advanced Oxidation Processes (AOPs) are promising technologies for the removal of organic compounds resistant to biological treatments. They include photocatalytic processes that involve the use of luminous radiation capable of electronically activating the catalyst; the energy content of this radiation must be in the visible or ultraviolet (UV) region. Moreover, the photocatalyst should be made of a semiconductor material with an electron structure capable of generating electron/hole pairs after irradiation at a given wavelength. The electron/hole pairs promote the formation of highly reactive radical species that participate in the pollutant degradation. These radicals result from reduction and oxidation reactions when promoted by the electron and by the positive hole generated, respectively (Ahmed et al., 2011; Rivera-Utrilla et al., 2012; Velo-Gala et al., 2013).

TiO_2 is one of the most widely used photocatalysts in water treatments, either alone or in combination with others that act as dopers and/or material supports (Ahmed et al., 2011; Leon and Radovic, 1994; Shan et al., 2010; Teh and Mohamed, 2011). However, there are drawbacks to the use of these materials, including the following: (i) their difficult removal from the treated effluent, (ii) the need for their recovery and reutilization, (iii) their reduced percentage solar spectrum radiation absorption, and (iv) their high electron/hole recombination level. Recent studies have centered on photocatalysis processes that reduce these shortcomings, including the preparation of semiconductors that have a large surface area or are placed on porous carbon materials (Baek et al., 2013; Cordero et al., 2007; Leary and Westwood, 2011; Li Puma et al., 2008; Lim et al., 2011; Rivera-Utrilla et al., 2012; Tryba et al., 2003). The textural and chemical properties of activated carbons improve the performance of photocatalytic processes when used as photocatalyst supports, largely attributable to the increased contact surface between photocatalyst and pollutant (Figueiredo and Pereira, 2010; Matos et al., 2009; Rodríguez-

Reinoso, 1998; Wang et al., 2007). In these cases, carbon plays a mere support function, although it was recently demonstrated (Haro et al., 2012; Velasco et al., 2012; Velasco et al., 2013) that activated carbons may act as photocatalysts under the action of UV light, which constitutes a new and promising approach to pollutant treatment. García-Cruz et al. (2014) studied the immobilization of nickel (Ni) on various carbon supports and its application as electrocatalyst to oxidize propargyl alcohol in alkaline medium. The results revealed the importance of the phase of the metal within the carbon structure, with nanoparticles Ni yielding the highest performances. The combined effect of UV radiation and carbon has been widely studied by Velo-Gala et al. (2013), who analyzed the effectiveness of four commercial carbons to remove sodium diatrizoate in the presence of UV radiation. The results demonstrated that the catalytic contribution exceeds 53% after 1 min of treatment. This catalytic activity is increased in samples with higher percentage surface oxygen, mainly when this is formed by ester/anhydride groups and carbon atoms with sp^2 hybridization.

There have been few studies on herbicide removal from water by photocatalysis (Andersen et al., 2013; Catastini et al., 2004; Mugadza and Nyokong, 2010; Watanabe et al., 2005). Orellana et al. (2016) analyzed AMT photocatalytic degradation in aqueous solution in the presence of organic aerogels and xerogels doped with different transition metals. The results suggest that the positive holes generated in the valence band and the electrons that promote the conduction band play an essential role in the mechanism by which xerogels promote AMT photodegradation. Band-gap energy values are closely related to the presence of ─C═O/─OH groups in the structure of the gels. Thus, Ni xerogel (X-Ni) has the highest ─C═O/─OH group content and photocatalytic activity.
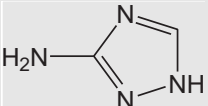
With this background, the objectives of the present study were as follows: to determine the influence of different operational variables on the photodegradation process, including the initial herbicide and catalyst concentrations, medium pH, ionic strength, natural organic matter (NOM), light intensity, and the presence of TiO_2; to analyze the time course of total organic carbon (TOC) and medium toxicity during AMT photodegradation with Ni xerogel; and to establish the influence of the type of water (ultrapure, tap, and wastewater). Determination of these parameters is essential for the correct design of technological applications of this photocatalytic process.

2. Materials and methods

2.1. Reagents

All chemical reagents used in this study (amitrole, hydrochloric acid, monobasic sodium phosphate, dibasic sodium phos-

Table 1 Chemical properties of amitrole.

Structure	Molecular formula	Molecular weight g/mol	Solubility in water mg/L	pK$_1$	pK$_2$
H_2N─ [triazole ring structure] ─NH	$C_2H_4N_4$	84.1	28×10^4	4.3	10.4

phate, sodium hydroxide, and phosphoric acid) were of high purity analytical grade and supplied by Sigma-Aldrich. All solutions were prepared with ultrapure water obtained with Milli-Q equipment (18.2 MΩ cm). Table 1 exhibits some chemical properties of AMT. The speciation diagram of AMT as a function of solution pH and its pK_a values was previously determined by potentiometric titration (Orellana et al., 2015). Thus, AMT can exist in protonated, neutral, or deprotonated state depending on the solution pH (virtually protonated at pH $\leqslant$ 3, neutral at pH 6–9, and completely deprotonated at pH $\geqslant$ 12), and its pK_a values are 4.3 and 10.4 (Orellana et al., 2015) (Table 1).

2.2. Materials

A nickel organic xerogel (X-Ni) was used for this study. The procedure for the preparation of X-Ni has been described elsewhere (Orellana et al., 2016). The organic gel was characterized by N_2 adsorption at $-196\,°C$ using an Autosorb 1 analyzer from Quantachrome. The BET surface area was 103 m^2/g, and its micropore volume was 0.040 cm^3/g with mean micropore width of 1.99 nm from DR and Stoeckli equations. The mesopore volume, obtained from the difference between the amount of N_2 adsorbed at a relative pressure of 0.95 and the micropore volume, was 0.295 cm^3/g. The pH of the point of zero charge (pH_{PZC}) of X-Ni was 3.4, obtained from potentiometric titrations (Orellana et al., 2016).

2.3. Photocatalytic degradation of AMT in the presence of X-Ni and/or TiO_2

The photoactivity of X-Ni under UV light was evaluated for AMT degradation in water. Experimental details have been reported elsewhere (Orellana-García et al., 2015, 2016). Briefly, the oxidation experiments were carried out using 0.7 L of a 0.30 mmol/L AMT solution in the presence of 250 mg/L of X-Ni. Solution pH was adjusted to the desired value by adding 0.1 mol/L NaOH or 0.1 mol/L HCl solutions. In each experiment, after stabilizing the lamp (a low-pressure [LP] mercury lamp) and controlling the temperature (25 °C), the photoreactor was turned on, and aliquots were withdrawn from the reactor at different time intervals in order to assess the herbicide concentration and TOC. Samples were immediately filtered with Millipore disk filters (0.45 μm) to remove the organic xerogel. Experiments were also carried out using a UV reactor system 2 (UV Consulting Peschl) provided with a medium-pressure (MP) mercury vapor lamp (TQ 150, nominal power 150 W).

2.4. Analytical methods

AMT concentrations in solution were determined by reversed-phase high performance liquid chromatography (HPLC) using a chromatograph (Thermo-Fischer) equipped with UV8000 photodiode detector. The chromatographic column was a Hypersil GOLD 250 × 4.6 mm. The mobile phase for AMT was water (pH = 6, using phosphate buffer) in isocratic mode at an elution flow rate of 1 mL/min. Injection volume was 20 μL in all samples. Detector wavelength was 202 nm.

AMT mineralization was followed by measurement of the medium TOC using a Shimadzu V-CSH analyzer with ASI-V autosampler and subtracting the inorganic carbon value in each sample from the total carbon value.

The superoxide radicals ($O_2^{\cdot-}$) generated were determined by reaction with tetranitromethane (TNM), evaluating the formation of nitroform anions ($C(NO_2)_3^-$), which were determined at 350 nm (Shao et al., 2010).

HO$^{\cdot}$ radical concentrations were measured by following their reaction with dimethyl sulfoxide to quantitatively form formaldehyde, which reacts with 2,4-dinitrophenylhydrazine, giving rise to the corresponding hydrazone, determined by HPLC-UV (Tai et al., 2004).

The toxicity of degradation products was assessed by means of the normalized biotest (UNE/EN/ISO 11348-2) of luminescent inhibition of Vibrio bacteria (NRRL B-11177) using the LUMIStox 300 system (Dr. Lange GmbH) with LUMIStherm incubator. The toxicity was defined as the percentage inhibition at 15 min of exposure. In all cases, the percentage inhibition was determined by comparing the response of an established control saline solution with that of the study sample.

The influence of the chemical composition of the water on herbicide photodegradation was studied in ultrapure water, tap water, and urban wastewater from the city of Jaen (Andalusia, Southern Spain). After characterization of these waters, they were filtered and refrigerated until use. Table 2 displays the characteristics of the water samples.

3. Results and discussion

According to the results obtained in a previous study (Orellana-García et al., 2016), the reduction in AMT concentration by photodegradation in the presence of Ni xerogel is attributable to three processes: (a) direct photolysis, (b) adsorption, and (c) synergic effect produced by the presence of the xerogel. Hence, AMT removal in the presence of X-Ni can be mathematically described by the following equation:

Table 2 Physicochemical characteristics of water samples.

Water	pH	TOC mg/L	T[a] (%)	[HCO_3^-] mg/L	[SO_4^{2-}] mg/L	[NO_3^-] mg/L	[Ca^{2+}] mg/L	[Mg^{2+}] mg/L
Ultrapure	6.1	0.0	100.0	0.0	0.0	0.0	0.0	0.0
Tap	8.0	0.0	99.1	245.0	10.2	12.5	86.1	11.2
Wastewater	8.1	14.2	68.9	290.6	97.6	25.3	119.9	11.2

[a] Transmittance (%) at 254 nm.

Table 3 Experimental conditions and kinetic parameters for AMT removal in the presence of Ni xerogel.

Exp. No.	[X-Ni] mg/L	pH	[AMT] mmol/L	[NaCl]	[GA]	$k_{OB}\cdot10^3$ min^{-1}	$k_{UV}\cdot10^3$ min^{-1}	$k_{ADS}\cdot10^3$ min^{-1}	$k_{SE}\cdot10^3$ min^{-1}	[a]AMT$_{UV/GEL}$ %	[a]SE$_{UV/GEL}$ %	[a]TOCAMT$_{UV/GEL}$ %	[a]TOCSE$_{UV/GEL}$ %
1	100	7	0.30	0		24.2	12.8	2.0	9.4	66.8	21.0	33.3	14.1
2	250	7	0.30	0		37.1	12.8	5.6	18.7	77.6	24.4	42.9	16.3
3	500	7	0.30	0		35.9	12.8	8.5	14.6	74.4	8.4	43.8	4.3
4	250	7	0.12	0		64.8	62.6	6.7	–	92.0	–	50.0	–
5	250	7	0.59	0		24.4	7.3	2.3	14.8	61.6	21.6	31.8	14.8
6	250	7	1.07	0		8.9	3.7	0.5	4.7	33.9	20.0	10.8	7.8
7	250	3	0.30	0		25.6	18.2	4.9	2.5	69.6	2.9	37.0	15.0
8	250	12	0.30	0		73.7	22.2	7.1	44.4	96.9	25.1	66.7	24.9
9	250	7	0.30	1		31.6	14.6	5.3	11.7	75.9	13.8	42.8	3.9
10	250	7	0.30	10		25.1	15.9	3.9	5.3	66.9	5.3	35.7	–
11	250	7	0.30	0	0.03	30.2	16.1	4.7	9.4	72.9	9.4	26.7	–
12	250	7	0.30	0	0.09	20.3	17.8	2.8	–	57.3	–	23.5	–
13	250	7	0.30	0	0.18	5.2	10.9	1.5	–	18.8	–	5.0	–

[a] 45 min of irradiation.

$$-V_{OB} = -\frac{[dAMT]}{dt} = -(V_{UV} + V_{ADS} + V_{SE})$$
$$= -(k_{UV} + k_{ADS} + k_{SE}) \cdot [AMT] \tag{1}$$

where k_{UV} is the AMT removal constant due to direct photolysis, k_{ADS} is the adsorption rate constant, and k_{SE} is the influence of the xerogel present in the medium on k_{OB} (synergic effect). Therefore, the calculation of k_{SE} requires separate determinations of the contributions of direct photolysis and adsorption.

The rate constant values for the different experimental conditions are listed in Table 3, which also include the percentage removal by synergic effect of X-Ni at 45 min irradiation. This value was calculated by subtracting the adsorptive and photolytic contributions from the total percentage removal in the UV/X-Ni system (Eq. (2)).

$$\%SE_{UV/GEL} = \%AMT_{UV/GEL} - \%AMT_{UV} - \%A_{GEL} \tag{2}$$

where $\%\,SE_{UV/GEL}$ is the percentage AMT removal due to the synergic effect produced by the presence of xerogel during exposure to UV radiation, $\%\,AMT_{UV/GEL}$ is the percentage total AMT degradation in the UV/X-Ni photocatalytic process, $\%\,AMT_{UV}$ is the percentage AMT degradation by direct photolysis, and $\%\,A_{GEL}$ is the percentage AMT degradation by adsorption on X-Ni. We discuss below the influence of the different experimental variables on AMT removal.

3.1. Influence of X-Ni concentration

In photocatalytic processes, the amount of photocatalyst is a key parameter that can affect the herbicide photodegradation rate. The effect of the baseline photocatalyst concentration on AMT removal kinetics was analyzed by conducting experiments at different X-Ni concentrations from 100 to 500 mg/L. Fig. 1 depicts the results obtained. AMT photodegradation kinetics (Fig. 1) were adjusted to a pseudo-first order kinetic model, obtaining the photocatalytic degradation constant, k_{OB}. Table 3 (Exp. Nos. 1–3) lists the values of kinetic parameters of AMT photodegradation as a function of the initial X-Ni concentration. Thus, it can be observed that k_{OB} is directly proportional to the baseline X-Ni concentration up to a maximum with a slight decrease thereafter, indicating progressive catalyst saturation of photon absorption at a given incident radiation flow. The results show that at concentrations close to 250 mg/L X-Ni, the AMT photodegradation rate is not affected by an additional increase in the initial X-Ni concentration (Fig. 2). This may be attributable to (i) aggregation of X-Ni particles at high concentrations, decreasing the number of active sites available for light absorption and thereby reducing the photodegradation rate (Parra et al., 2004), and (ii) increase in light dispersion and consequent reduction in its penetration through the solution, given the excess concentration of particles in suspension (Parra et al., 2004; Fenoll et al., 2012). A rise in the catalyst dose increases the number of active adsorption sites, with a percentage AMT of 5% at 45 min of irradiation with a catalyst dose of 100 mg/l and 26% with a dose of 500 mg/L; likewise, the adsorption rate constant also rises from 2.0×10^{-3} to 8.5×10^{-3} min^{-1} (Table 3). The balance between these opposed phenomena results in an optimal catalyst dose for the photocatalytic reaction (Adesina, 2004), in the present case one of around 250 mg/L, which yields the highest k_{OB} and k_{SE} values and per-
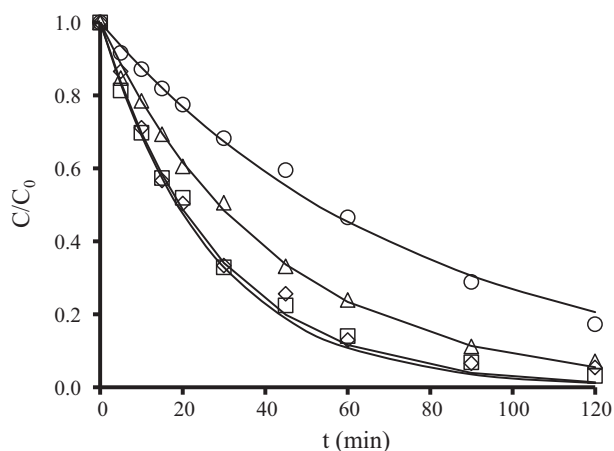
Figure 1   AMT photodegradation as a function of irradiation time at different initial catalyst (X-Ni) concentrations. pH = 7, [AMT] = 0.30 mmol/L. (○) Direct photolysis; (△) 100 mg/L; (□) 250 mg/L; (◇) 500 mg/L.
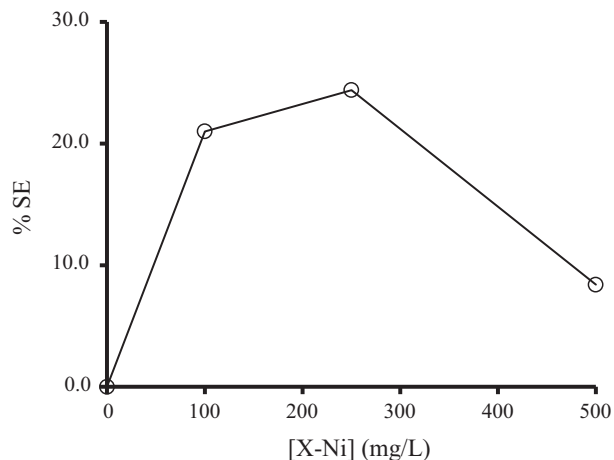
Figure 2   Variation of synergic effect as a function of initial X-Ni concentration at 45 min of irradiation. pH = 7, [AMT] = 0.30 mmol/L.

centage $AMT_{UV/GEL}$, $SE_{UV/GEL}$, and $TOCSE_{UV/GEL}$ degradation (Table 3).

The proposed mechanism to explain the photoactivity of nickel organic xerogel was previously described (Orellana-García et al., 2016). In brief, the presence of xerogels during AMT photodegradation promotes the generation of superoxide and hydroxyl radicals through the photogeneration of electron-positive gap pairs. Figure SM 1 depicts the time course of HO$^{\bullet}$ and O$_2^-$ radicals as a function of the catalyst dose added. It can be observed that the concentration of both radicals increases with higher doses of added matter. We also highlight the elevated oxygen consumption, with complete dissolved oxygen removal (regardless of the catalyst mass) at 45 min of treatment.

Investigation of catalyst reuse and stability is very important for evaluating its applicability for industrial and real wastewater treatment. Figure SM 2 shows the evolution of

AMT removal with time for four consecutive photocatalytic runs performed with the same catalyst sample, recovered by filtration and thoroughly washed with water, after each cycle. As can be seen in this figure, only few differences are observed among the four cycles, and AMT removal slightly dropped from 96.9% to 93.1% in the fourth consecutive cycle, less than 4% loss of catalyst activity. These results indicate that the X-Ni catalyst exhibits a high efficiency under consecutive runs.

3.2. Influence of AMT concentration

The effect of the initial AMT concentration on photodegradation was analyzed by using initial concentrations ranging between 0.12 and 1.07 mmol/L. Figure SM 3 in Supplementary Material shows AMT photodegradation kinetics as a function of initial concentration. Table 3 exhibits the kinetic parameters (Exp. Nos. 2, 4–6), showing that k_{OB} values decrease from 64.8×10^{-3} to 8.9×10^{-3} min^{-1} when the initial AMT concentration increases from 0.12 to 1.07 mmol/L. Results obtained indicate that increasing numbers of herbicide molecules are adsorbed on the photocatalyst surface with the rise in herbicide concentration but the AMT degradation rate decreases. This may be due to the following: (i) the generation of intermediate compounds that can be adsorbed on the catalyst surface, deactivating the active photocatalyst sites (Bahnemann et al., 2007) and (ii) the higher concentrations of degradation compounds generated, producing a greater consumption of oxidizing species in the catalytic photodegradation process (Ahmed et al., 2011).

Results indicate that the percentage degradation at 45 min irradiation is also reduced at higher AMT initial concentrations, decreasing from 92% to 33.9% with a rise in the initial concentration from 0.12 to 1.07 mmol/L, which is also accompanied by a reduction in the percentage mineralization from 50.0% to 10.8%. These results indicate that by-products are not mineralized to the desired extent, with by-products that have a lower molecular weight than AMT remaining in the medium during the treatment. Interestingly, the order of variation of the rate constant, k_{SE}, is the same as that of k_{OB}.
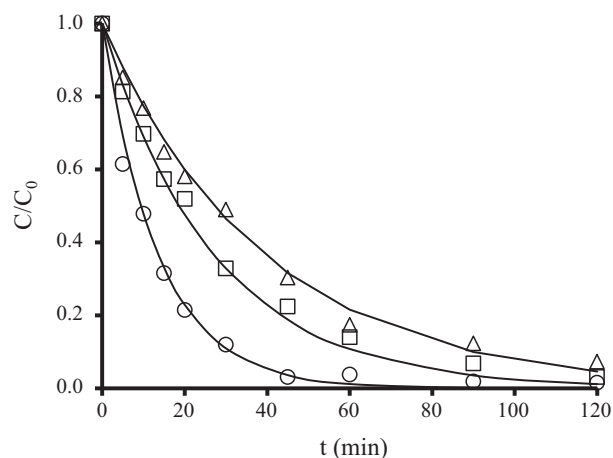
Figure 3   Effect of pH on AMT photodegradation. [AMT] = 0.30 mmol/L, [X-Ni] = 250 mg/L. (△) pH 3; (□) pH 7; (○) pH 12.

According to the present findings, an appreciable synergic effect requires a minimum pollutant concentration of 0.59 mmol/L, whereas AMT is removed by photolysis and adsorption alone at lower concentrations.

3.3. Influence of pH

The influence of solution pH on AMT photodegradation was analyzed by conducting experiments with pH values between 3 and 12, selected according to the pK_a values (Table 1) and AMT species distribution diagram (Orellana-García et al., 2015). Fig. 3 depicts AMT degradation kinetics at different pH values, and Table 3 exhibits the corresponding kinetic parameters (Exp. Nos. 2, 7, and 8). Results indicate that AMT photolysis is highly pH-dependent and is generally favored at pHs in which AMT is in ionic form. Thus, $k_{UV} = 12.8 \times 10^{-3}$ min^{-1} at pH 7, 18.2×10^{-3} min^{-1} at pH 3, and 22.2×10^{-3} min^{-1} at pH 12. However, the photodegradation constant, k_{OB}, increases from 25.6×10^{-3} min^{-1} at pH 3 to 73.7×10^{-3} min^{-1} at pH 12. There is also higher degradation (96.9%) and mineralization (66.7%) at pH 12. The same trend is observed for $SE_{UV/GEL}$ and $TOCSE_{UV/GEL}$ values, with $SE_{UV/GEL}$ of 2.9% and $TOCSE_{UV/GEL}$ of 15% at pH 3 versus $SE_{UV/GEL}$ of 25.1% and $TOCSE_{UV/GEL}$ of 24.9% at pH 12. It should also be noted that at 45 min of reaction, the amounts adsorbed increase from 2.9 mg/L at pH 3 to 3.2 mg/L at pH 7 and 3.4 mg/L at pH 12.

The increased AMT degradation rate in alkaline conditions can be attributed to a higher HO$^{\bullet}$ radical generation due to the presence of more OH$^-$ ions on the catalyst surface. At pH 12, X-Ni is negatively charged ($pH_{PZC} = 3.4$), and there is a large amount of OH$^-$ in the medium. Elevated OH$^-$ concentrations would increase the scavenging of photogenerated holes and yield highly oxidative HO$^{\bullet}$ species through Eq. (3) (Wei et al., 2009).

$$OH^- + h^+ \rightarrow HO^{\bullet} \qquad (3)$$

In contrast, the catalyst surface is positively charged at pH 3, and the degradation reaction mainly results from photogenerated holes, whose oxidizing capacity is somewhat lower than that of HO$^{\bullet}$ species (Wei et al., 2009; Wu et al., 2009).

3.4. Influence of chloride anions in the medium

Natural waters are complex matrixes containing anions such as chlorides, which can interfere with photocatalytic AMT degradation by reacting with the radical species formed during photocatalysis. This effect was analyzed by adding increasing amounts of NaCl (1–10 mmol/L) to 0.30 mmol/L AMT solutions. Results are displayed in Table 3 (Exp. Nos. 2, 9, and 10) and Figure SM 4 in Supplementary Material. Experimental

results demonstrate that an increased NaCl concentration has an inhibitory effect, reducing the photodegradation rate constant (k_{OB}) from 37.1×10^{-3} min^{-1} to 25.1×10^{-3} min^{-1} in the absence and presence of 10 mmol/L NaCl, respectively. This inhibitory effect is also observed for $SE_{UV/GEL}$ and TOC. This effect of the chloride anion can be explained by the reaction of positive holes and HO$^{\bullet}$ radicals with the chloride anions, which behave as scavengers of h$^+$ and HO$^{\bullet}$ radicals in agreement with reactions (4) and (5), reducing photocatalytic AMT mineralization (Chen et al., 2010; Wu et al., 2009).

$$Cl^- + h^+ \rightarrow Cl^{\bullet} \qquad (4)$$

$$HO^{\bullet} + Cl^- \rightarrow OH^- + Cl^{\bullet} \qquad (5)$$

The chloride atoms generated have a lower reactivity in comparison with the positive holes and HO$^{\bullet}$ radicals (Chen et al., 2010; Mahmoodi et al., 2007).

3.5. Influence of the presence of NOM in the medium

NOM is generally present in natural waters, and its effect on AMT degradation was analyzed by using gallic acid (GA), structural unit of NOM, as reference substance. Increasing amounts of GA, ranging from 0.03 to 0.18 mmol/L, were added to solutions of 0.30 mmol/L AMT. Figure SM 5 in Supplementary Material depicts the photodegradation kinetics of AMT in the presence and absence of GA. Table 3 (Exp. Nos. 2, 11–13) exhibits the values of AMT photodegradation
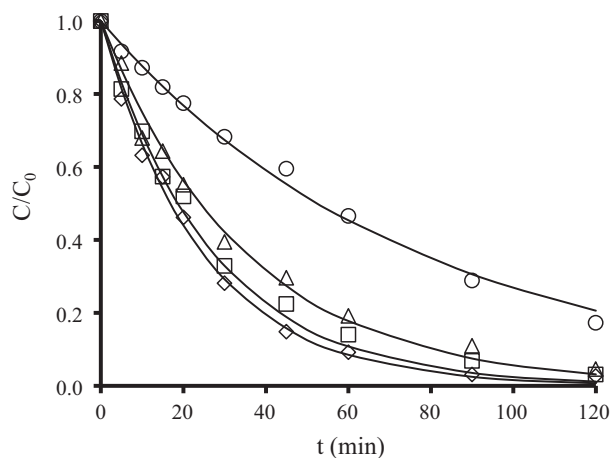
Figure 4 Comparison of AMT photodegradation in the presence of different photocatalysts. pH = 7, [AMT] = 0.30 mmol/L, [Catalyst] = 250 mg/L. (○) Direct photolysis; (△) TiO$_2$; (□) X-Ni; (◇) X-Ni/TiO$_2$.

Table 4 Influence of the water matrix and type of lamp on AMT removal. [AMT] = 0.30 mmol/L, [X-Ni] = 250 mg/L, pH = 7.

Exp. No.	Water matrix	Lamp	$k_{OB} \cdot 10^3$ min^{-1}	$k_{UV} \cdot 10^3$ min^{-1}	$k_{ADS} \cdot 10^3$ min^{-1}	$k_{SE} \cdot 10^3$ min^{-1}	$AMT_{UV/GEL}$ %	$SE_{UV/GEL}$ %	[a]$TOCAMT_{UV/GEL}$ %	[a]$TOCSE_{UV/GEL}$ %
2	Ultrapure	LP	37.1	12.8	5.6	18.7	77.6	24.4	42.9	16.3
14	Tap	LP	19.0	6.6	3.0	9.4	54.1	23.0	27.8	12.8
15	Waste	LP	9.7	4.1	2.5	3.1	36.3	14.3	21.1	10.0
16	Ultrapure	MP	42.0	17.0	5.6	19.4	81.2	15.1	55.6	23.9

[a] 45 min of irradiation.

kinetic parameters at different baseline GA concentrations. The photodegradation rate constant (k_{OB}) decreases at higher GA concentrations, and the addition of large amounts of GA to the medium eliminates the synergic effect. These results are explained by the following: (i) a reduction in light transmission and therefore in photocatalytic degradation rate with increased GA concentrations, and (ii) competition between GA and AMT both for the highly oxidizing radicals generated in the solution in photodegradation (Lin and Lin, 2007) and for the adsorption centers on the xerogel surface in adsorption.

3.6. Influence of light intensity

Light intensity determines the degree of light adsorption by the photocatalyst at a given wavelength. The formation of electron-positive hole pairs in the photochemical reaction is highly dependent on this intensity (Cassano and Alfano, 2000).

Figure SM 6 in Supplementary Material depicts the AMT photodegradation kinetics obtained with the LP and MP mercury lamps. Table 4 exhibits the kinetic parameters (Exp. Nos. 2 and 16). As observed, k_{OB} values increase from 37.1×10^{-3} with LP lamp ($\lambda = 254$ nm) to 42.0×10^{-3} min^{-1} with MP lamp (150 W). AMT degradation effectiveness is slightly higher under irradiation with MP lamp (81.2%) versus LP lamp (77.6%). Increased irradiated light intensity on the solution produces a higher electron/hole pair photogeneration rate on the catalyst surface, increasing the oxidation capacity of the system. Chen et al. (2007) reported similar results for dimethoate degradation.

3.7. Influence of the presence of TiO$_2$

Fig. 4 depicts AMT photodegradation kinetics in the presence of X-Ni, TiO$_2$, and X-Ni/TiO$_2$ combined, alongside the direct photolysis results. Degradation is faster in the presence of X-Ni/TiO$_2$ than in the presence of X-Ni or TiO$_2$ alone. The percentage AMT adsorption on X-Ni at 45 min is 12.7%, compared with no adsorption in the case of TiO$_2$ and 7.6% using X-Ni/TiO$_2$. The amounts of catalyst were 250 mg/L in the X-Ni system and 125 mg/L X-Ni with 125 mg/L TiO$_2$ in the X-Ni/TiO$_2$ system. Although the percentage adsorption is lower with the X-Ni/TiO$_2$ system, the AMT degradation is faster (Table 5).

Table 5 exhibits the kinetic parameters and the percentage degradation and mineralization values for the studied systems. Percentage AMT removal is 77.6, 70.4, and 85.1% in the presence of X-Ni, TiO$_2$, and X-Ni/TiO$_2$, respectively. AMT removal by direct photolysis is 40.5% at 45 min of irradiation. According to these results, AMT removal is due to the combined effects of adsorption and catalytic oxidation.

Table 5 shows that rate constant, k_{OB}, is higher with X-Ni (37.1×10^{-3} min^{-1}) than with TiO$_2$ (28.9×10^{-3} min^{-1}) and is highest with the X-Ni/TiO$_2$ combination (41.0×10^{-3} min^{-1}), which is therefore the most active system. This increased photoactivity is due to the increased synergic effect of the presence of both materials. This effect was evaluated during the reaction by determining synergic factor R (Eq. (6)), based on the comparison among AMT degradation rate constants (k_{OB}) by adsorption, direct photolysis, and photocatalysis (Gu et al., 2010; Matos et al., 2013):

$$R = \frac{k_{OB}}{k_{UV} + k_{ADS}} \tag{6}$$

The R value for X-Ni is 2.0, evidencing a significant synergic effect due to interaction between UV radiation and X-Ni particles. The R value for the X-Ni/TiO$_2$ system is 2.6, indicating a higher synergic effect.

The AMT removal rate is much higher with the X-Ni/TiO$_2$ combination than with the X-Ni or TiO$_2$ system alone. This may be attributable to the presence of surface carboxylic acid groups on X-Ni, as confirmed in a previous study using a UV/TiO$_2$/activated carbon system (Rivera-Utrilla et al., 2012). Accordingly, carboxylic acid groups act as catalytic reaction centers, capturing dissolved electrons from the photoactivation of TiO$_2$. This reaction reduces carboxylic acid and ketone and generates H$_2$O$_2$, which is decomposed into HO$^•$ radicals, while the ketone generated is subsequently transformed into a surface alcohol group, giving rise to additional HO$^•$ radicals (Rivera-Utrilla et al., 2012).

3.8. Influence of the water matrix

The influence of the water matrix on AMT photodegradation in the presence of X-Ni was analyzed by conducting experiments with waters of different chemical compositions (Table 2). Wastewaters have higher TOC and electrolyte content and lower transmittance. Fig. 5 depicts the AMT photodegradation kinetics as a function of water type. Table 4 (Exp. Nos. 2, 14, and 15) lists the rate constants and percentage degradation and mineralization values obtained in the studied waters. k_{OB} and k_{SE} values decrease in the order ultrapure water > tap water > urban wastewater. The highest percentage AMT degradation (24.4%) and mineralization (16.3%) due to the synergic effect are obtained in ultrapure water.

These findings are largely explained by the presence in tap and wastewater of inorganic anions and NOM, which compete for the radicals generated in photocatalysis (Orellana-García et al., 2015). This reduces the availability of oxidizing radical species to interact with AMT, giving rise to lower percentage degradation. Wastewater has the lowest light transmittance,

Table 5 Comparison of X-Ni with TiO$_2$-P$_{25}$ and X-Ni/TiO$_2$-P$_{25}$ mixture for AMT removal. [AMT] = 0.30 mmol/L, pH = 7.

Exp. No.	Materials	$k_{OB} \cdot 10^3$ min^{-1}	$k_{UV} \cdot 10^3$ min^{-1}	$k_{ADS} \cdot 10^3$ min^{-1}	[a]AMT$_{UV/GEL}$ %	[a]TOCAMT$_{UV/GEL}$ %
2	X-Ni	37.1	12.8	5.6	77.6	42.9
17	TiO$_2$-P$_{25}$	28.9	12.8	0.0	70.4	32.1
18	X-Ni/TiO$_2$	41.0	12.8	3.0	85.1	45.0

[a] 45 min of irradiation.
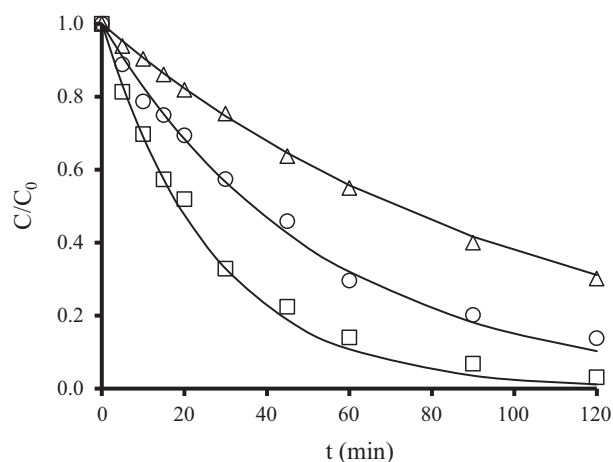
Figure 5 Influence of the type of water on AMT photodegradation. pH = 7, [AMT] = 0.30 mmol/L, [X-Ni] = 250 mg/L. (□) Ultrapure; (○) tap water; (△) wastewater.
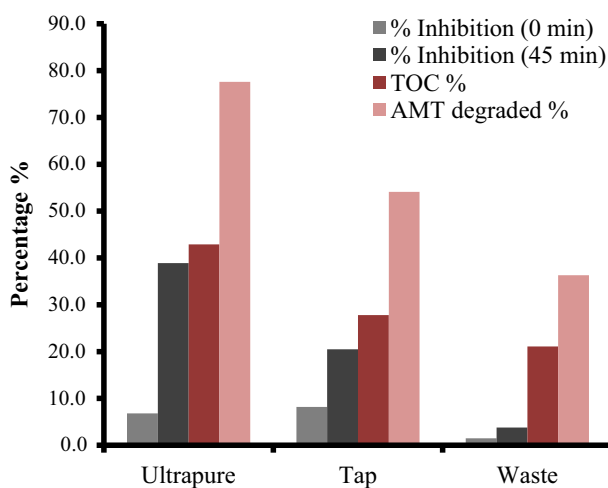
Figure 6 Initial toxicity and toxicity after 45 min of irradiation in different types of water. [AMT] = 0.30 mmol/L, [X-Ni] = 250 mg/L.

absorbing UV radiation and considerably reducing the number of photons that reach the catalyst surface. These results confirm that organic matter in wastewaters acts as UV light filter, reducing the effectiveness of the treatment for AMT removal from the medium.

At 45 min of irradiation, the percentage AMT degradation is always higher than the percentage TOC removal, indicating that not all of the degraded AMT is mineralized during photocatalytic degradation in any of the studied waters. The residual TOC that remains in the medium is due to the presence of degradation by-products that have not transformed into CO_2 (Orellana-García et al., 2015).

Fig. 6 depicts the AMT toxicity in all study waters alongside the percentage AMT degradation and TOC removal. Baseline percentage inhibition for 0.30 mmol/L AMT is 6.8% in ultrapure water, 8.1% in tap water, and 1.8% in wastewater. At 45 min of treatment in ultrapure water,

77.6% ATM is degraded and 42.9% of the initial AMT concentration is mineralized, while the toxicity increases from 6.8% to 38.9%. In wastewater, 36.3% AMT is degraded and 21.1% of the initial AMT concentration is mineralized, while the toxicity rises from 1.8% to 3.8%. The lower toxicity in wastewater than in ultrapure water is due to the lower percentage AMT degradation, which generates fewer by-products. As observed in Fig. 6, the toxicity increases with longer treatment time in all three types of water, indicating the formation of by-products that are smaller than AMT and can more readily penetrate the cell.

With the analysis of the above operational parameters on the AMT photodegradation process, the best experimental conditions can be established. In brief, the variables that favor the AMT degradation rate are as follows: an increase in the initial X-Ni concentration up to a maximum of 250 mg/L, pH values at which AMT is in its ionic form, an increase in the irradiated light intensity on the solution and the presence of TiO₂. Conversely, increased pollutant concentration, the presence of chloride or organic matter in the medium causes a decrease in the degradation rate.

4. Conclusions

The AMT degradation rate is directly proportional to the initial X-Ni concentration up to a maximum of around 250 mg/L with a slight decrease thereafter, indicating the progressive saturation of photon absorption on the catalyst for a given incident radiation flow.

The stability of the catalyst used was evaluated during consecutives cycles proving the relatively good stability of the X-Ni since only a slight decrease in catalytic activity was observed.

AMT photolysis is highly pH-dependent and is generally favored by a pH at which AMT is in ionic form. The increased AMT degradation rate in alkaline conditions is attributable to a greater generation of HO˙ radicals due to the high concentration of OH⁻ ions on the catalyst surface. The presence of chlorides reduces the AMT degradation rate, because Cl⁻ anions behave as h⁺ and HO˙ radical scavengers. The degradation rate is also decreased by the addition of organic matter, which acts as a filter and reduces the radiation reaching the X-Ni. In addition, GA in the medium competes for active adsorption sites and for the highly oxidizing radical species generated during photodegradation.

TOC removal kinetics during AMT degradation in the presence of X-Ni are similar to the AMT degradation kinetics.

Finally, we highlight that AMT photodegradation is more effective in ultrapure water than in wastewater or tap water. In all systems, the optimal catalyst concentration is 250 mg/L. The toxicity increases with longer treatment time, indicating the formation of by-products that are smaller than AMT and can more readily penetrate the cell.

Appendix A. Supplementary material

Supplementary data associated with this article can be found, in the online version, at http://dx.doi.org/10.1016/j.arabjc.2016.10.005.

References

Adesina, A.A., 2004. Catal. Surv. Asia 8, 265–273.

Ahmed, S., Rasul, M.G., Brown, R., Hashib, M.A., 2011. J. Environ. Manage. 92, 311–330.

Andersen, J., Pelaez, M., Guay, L., Zhang, Z., O'Shea, K.N., Dionysiou, D.D., 2013. J. Hazard. Mater. 260, 569–575.

Baek, M.H., Jung, W.C., Yoon, J.W., Hong, J.S., Lee, Y.S., Suh, J.K., 2013. J. Ind. Eng. Chem. 19, 469–477.

Bahnemann, W., Muneer, M., Haque, M.M., 2007. Catal. Today 124, 133–148.

Cassano, A.E., Alfano, O.M., 2000. Catal. Today 58, 167–197.

Catastini, C., Rafqah, S., Mailhot, G., Sarakha, M., 2004. J. Photochem. Photobiol., A 162, 97–103.

Chen, J., Wang, D., Zhu, M., Gao, C., 2007. Desalination 207, 87–94.

Chen, J.Q., Hu, Z.J., Wang, D., Gao, C.J., Ji, R., 2010. Desalination 258, 28–33.

Cordero, T., Duchamp, C., Chovelon, J.M., Ferronato, C., Matos, J., 2007. J. Photochem. Photobiol., A 191, 122–131.

Da Pozzo, A., Merli, C., Sirés, I., Garrido, J.A., Rodríguez, R.M., Brillas, E., 2005. Environ. Chem. Lett. 3, 7–11.

Fenoll, J., Hellína, P., Martínez, C.M., Flores, P., Navarro, S., 2012. J. Photochem. Photobiol., A 238, 81–87.

Figueiredo, J.L., Pereira, M.F.R., 2010. Catal. Today 150, 2–7.

García-Cruz, L., Sáez, A., Ania, C.O., Solla-Gullón, J., Thiemann, T., Iniesta, J., Montiel, V., 2014. Carbon 73, 291–302.

Gu, L., Chen, Z., Sun, C., Wei, B., Yu, X., 2010. Desalination 263, 107–112.

Haro, M., Velasco, L.F., Ania, C.O., 2012. Catal. Sci. Technol. 11, 2264–2272.

Leary, R., Westwood, A., 2011. Carbon 49, 741–772.

Leon, C.A., Radovic, L.R., 1994. Interfacial chemistry and electro-chemistry of carbon surfaces. In: Thrower, P.A. (Ed.), Chemistry and Physics of Carbon 24. Marcel Dekker, New York, pp. 213–310.

Li Puma, G., Bono, A., Krishnaiah, D., Collin, J.G., 2008. J. Hazard. Mater. 157, 209–219.

Lim, T.T., Yap, P.S., Srinivasan, M., Fane, A.G., 2011. Crit. Rev. Environ. Sci. Technol. 41, 1173–1230.

Lin, C., Lin, K., 2007. Chemosphere 66, 1872–1877.

Mahmoodi, N.M., Arami, M., Limaee, N.Y., Gharanjig, K., 2007. J. Hazard. Mater. 145, 65–71.

Matos, J., García, A., Cordero, T., Chovelon, J.M., Ferronato, C., 2009. Catal. Lett. 130, 568–574.

Matos, J., Hofman, M., Pietrzak, R., 2013. Carbon 54, 460–471.

Mugadza, T., Nyokong, T., 2010. Electrochim. Acta 55, 2606–2613.

Oesterreich, T., Klaus, U., Volk, M., Neidhart, B., Spiteller, M., 1999. Chemosphere 38, 379–392.

Orellana-García, F., Álvarez, M.A., López-Ramón, M.V., Rivera-Utrilla, J., Sánchez-Polo, M., 2015. Chem. Eng. J. 267, 182–190.

Orellana-García, F., Álvarez, M.A., López-Ramón, M.V., Rivera-Utrilla, J., Sánchez-Polo, M., 2016. Appl. Catal. B: Environ. 181, 94–102.

Parra, S., Stanca, S.E., Guasaquillo, I., Thampi, K.R., 2004. Appl. Catal. B: Environ. 51, 107–116.

Rivera-Utrilla, J., Sánchez-Polo, M., Abdel daiem, M.M., Ocampo-Pérez, R., 2012. Appl. Catal. B: Environ. 126, 100–107.

Rodríguez-Reinoso, R., 1998. Carbon 36, 159–175.

Shan, A.Y., Ghazi, T.I.M., Rashid, S.A., 2010. Appl. Catal. A: Gen. 389, 1–8.

Shao, J., Geacintov, N.E., Shafirovich, V., 2010. J. Phys. Chem. B 114, 6685–6692.

Tai, C., Peng, J.F., Liu, J.F., Jiang, G.B., Zou, H., 2004. Anal. Chim. Acta 527, 73–80.

Teh, C.M., Mohamed, A.R., 2011. J. Alloys Compd. 509, 1648–1660.

Tryba, B., Morawski, A.W., Inagaki, M., 2003. Appl. Catal. B: Environ. 41, 427–433.

Velasco, L.F., Fonseca, I.M., Parra, J.B., Lima, J.C., Ania, C.O., 2012. Carbon 50, 249–258.

Velasco, L.F., Maurino, V., Laurenti, E., Fonseca, I.M., Lima, J.C., Ania, C.O., 2013. Appl. Catal. A: Gen. 452, 1–8.

Velo-Gala, I., López-Peñalver, J.J., Sánchez-Polo, M., Rivera-Utrilla, J., 2013. Appl. Catal. B: Environ. 142, 694–704.

Wang, W., Silva, C.G., Faria, J.L., 2007. Appl. Catal. B: Environ. 70, 470–478.

Watanabe, N., Horikoshi, S., Kawasaki, A., Hidaka, H., 2005. Environ. Sci. Technol. 39, 2320–2326.

Wei, L., Shifu, C., Wei, Z., Sujuan, Z., 2009. J. Hazard. Mater. 164, 154–160.

Wu, R., Chena, C., Chen, M., Lu, C., 2009. J. Hazard. Mater. 162, 945–953.